Scattering and Diffraction of Elastodynamic Waves in a Concentric Cylindrical Phantom for MR Elastography

Benjamin L. Schwartz*, Ziying Yin, Temel K. Yaşar, Yifei Liu, Altaf A. Khan, Allen Q. Ye, Thomas J. Royston, and Richard L. Magin, *Fellow, IEEE*

***Abstract*—*Aim*: The focus of this paper is to report on the design and construction of a multiply connected phantom for use in magnetic resonance elastography (MRE)—an imaging technique that allows for the noninvasive visualization of the displacement field throughout an object from externally driven harmonic motion—as well as its inverse modeling with a closed-form analytic solution which is derived herein from first principles. *Methods*: Mathematically, the phantom is described as two infinite concentric circular cylinders with unequal complex shear moduli, harmonically vibrated at the exterior surface in a direction along their common axis. Each concentric cylinder is made of a hydrocolloid with its own specific solute concentration. They are assembled in a multistep process for which custom scaffolding was designed and built. A customized spin-echo-based MR elastography sequence with a sinusoidal motion-sensitizing gradient was used for data acquisition on a 9.4 T Agilent small-animal MR scanner. Complex moduli obtained from the inverse model are used to solve the forward problem with a finite-element method. *Results*: Both complex shear moduli show a significant frequency dependence ($p < 0.001$) in keeping with previous work. *Conclusion*: The novel multiply connected phantom and mathematical model are validated as a viable tool for MRE studies. *Significance*: On a small enough scale much of physiology can be mathematically modeled with basic geometric shapes, e.g., a cylinder representing a blood vessel. This study demonstrates the possibility of elegant mathematical analysis of phantoms specifically designed and carefully constructed for biomedical MRE studies.**

***Index Terms*—Cylindrical waves, MR elastography, viscoelastic media, cylindrical waves.**

I. Introduction

THE mechanical properties of biologic tissue are often correlated to their relative states of health. A malignant tumor in, e.g., breast, liver, pancreas, etc., tissue is noticeably stiffer than the surrounding healthy regions of that tissue. Further, the progression of disease can be characterized by the degree to which the mechanical properties veer from normal, e.g., the maturity of a blood clot in deep vein thrombosis [1]. This phenomenon makes the ancient art of palpation, the manual pressured probing of a patient's body, an invaluable method to detect maladies. Though inexpensive and universally applicable, noninvasive palpation is limited to the periphery of a patient's body. A small tumor deeply embedded in tissue could be missed, and allowed to grow, reducing a patient's chance of survival. Moreover, a doctor's tactile sensitivity to variations in tissue stiffness is, by nature, a subjective trait, prone to error in disease detection and characterization. The broad engineering challenge is centered around the noninvasive, high resolution, characterization of soft tissues through their mechanical behavior. Linear elastic theory defines a mechanical system through a plethora of parameters though an imaging modality need not consider them all to be clinically relevant. The complex shear modulus, in particular, has received scrutiny in the literature of late as a biomarker for pathologies in magnetic resonance (MR) elastography [2]–[5]. In an MR elastography, an object is perturbed with harmonic oscillations from a mechanical actuator. The displacement throughout the material, i.e., the wave field, is encoded in the phase of the MR signal by synchronizing the oscillation of the field from the gradient coils of the MRI scanner with the oscillatory frequency of the actuator. The shear modulus can be estimated from these wave data with various inverse modeling techniques [6]. Medical imaging requires phantom studies for validation. Hydrocolloid suspensions are affordable and easily made [7] making them ideal for use as tissue-mimicking phantoms in elastographic studies.

A. Homogeneous Material

To validate a novel technique or model in elastographic imaging, it is sometimes necessary that the samples being studied be homogeneous to eliminate artifacts from, e.g., scattering. Perriñez *et al.* used a bean curd (tofu) to mimic soft poroelastic tissue in MR elastography [8], estimating shear modulus from simulated data with a finite-element-based nonlinear inversion scheme. Othman *et al.* used agarose gel phantoms to extend MR elastography to the micro scale [9], [10]. Homogeneous gelatin phantoms have also been used in ultrasound elastography. Amador *et al.* validated their shear wave dispersion ultrasound vibrometry technique with a hydrocolloid mixture of gelatin, glycerol and cellulose by comparing the results to those of indentation tests [11], while Zhang *et al.* validated their surface wave method in a similar study [12]. Riek *et al.*

Manuscript received June 5, 2015; accepted February 5, 2016. Date of publication February 11, 2016; date of current version October 18, 2016. This research was supported by grants from the National Institute of Health (Nos. EB012142 and EB007537). *Asterisk indicates corresponding author.*

*B. L. Schwartz is with the Department of Bioengineering, University of Illinois at Chicago, Chicago, IL 60607 USA (e-mail: BenjiTheGreat@asu.edu).

Z. Yin, A. Q. Ye, T. J. Royston, and R. L. Magin are with the Department of Bioengineering, University of Illinois at Chicago.

T. K. Yaşar, Y. Liu, and A. A. Khan are with the Department of Mechanical and Industrial Engineering, University of Illinois at Chicago.

Color versions of one or more of the figures in this paper are available online at http://ieeexplore.ieee.org.

Digital Object Identifier 10.1109/TBME.2016.2527825

presented results on wide-range (200–800 Hz) magnetic resonance elasography (MRE) in agarose gels and human tissues using a frequency-dependent fractional order element—the so-called springpot—in their model [13].

B. Heterogeneities and Connectedness

Some researchers deliberately introduce heterogeneities in their phantoms to more closely mimic a biologic system. Petrov *et al.* investigated complex heterogenous geometries (using tofu and gelatin phantoms) in low-range ($<$125 Hz) multifrequency MRE and a nonlinear inversion optimization method [14], not unlike Perriñez *et al.* They used a Rayleigh damping material model to estimate complex viscoelastic parameters. Henni *et al.* did ultrasound elastography on a cuboidal gelatin phantom that had a soft cylindrical region running through it to validate their elegant analytic model of scattering and diffraction of a plane shear wave by an infinite cylinder [15]. Schmitt *et al.* used Henni's model to solve the inverse problem of characterizing vascular behavior with ultrasound elastography [16], [17]. Doyley *et al.* constructed elastically heterogeneous phantoms by embedding hydrogel spheres in a hydrogel medium of a different stiffness from the spheres to show that more sophisticated mathematical assumptions, i.e., nonlinearity, anisotropy, and viscoelasticity should be made when reconstructing elastograms from MR elastography data [18]. Qin *et al.* immersed spandex fibers in a polyvinyl alcohol hydrogel to test a combined MR elastography and diffusion tensor imaging technique [19]. Yin *et al.* designed a ball-in-tube phantom to demonstrate their novel technique for simultaneous acquisition of diffusion and MR elastography data [20]. As the geometry of the phantoms increases in complexity, e.g., being multiply connected as opposed to simply connected or mixing geometry, so do the analytic solutions describing their dynamic mechanical behavior. Certainly a phantom that accurately models the geometry of a brain would necessitate a technique like local frequency estimation [21] to infer its mechanical properties. But, there are many geometric configurations with clinical or academic relevance that are amenable to analytic solutions. Khan *et al.* modeled a corneal phantom as a thin viscoelastic plate [22]. They obtained an elastogram by fitting their closed form analytic solution to displacement data. Yasar *et al.* pioneered the technique of geometrically focusing the incident shear wave [23], and used the solution to a longitudinally vibrating, homogeneous, infinite circular cylinder to obtain shear stiffnesses of cylindrical phantoms over a wide range of frequencies [24], while Liu *et al.* investigated an even wider frequency range [25]. Okamoto *et al.* conducted a similar study but varied their phantoms' composition [26]. Also, they had a different mathematic solution because their actuation came from within their phantom, whereas Yasar *et al.* perturbed their phantom's outer surface.

C. Objective

Of all the works mentioned, Okamoto *et al.* is the only MR elastography study to obtain estimates of the complex shear modulus of a multiply connected body by inverse modeling with a closed form analytic solution. To our knowledge, there has been no such modeling of a multiply connected *heterogeneous* body in MR elastography and this is what we present now. We derive, from first principles, the solution to a concentric cylindrical body undergoing harmonic oscillations. We then describe the phantom construction, experimental procedure, parameter estimation, and the forward problem. To validate our model, we use the shear moduli estimates as inputs to solve the forward problem with a finite-element model (FEM) and compare that with experimental results. Finally we consider the immediate consequences of this work as well its implications for future research.

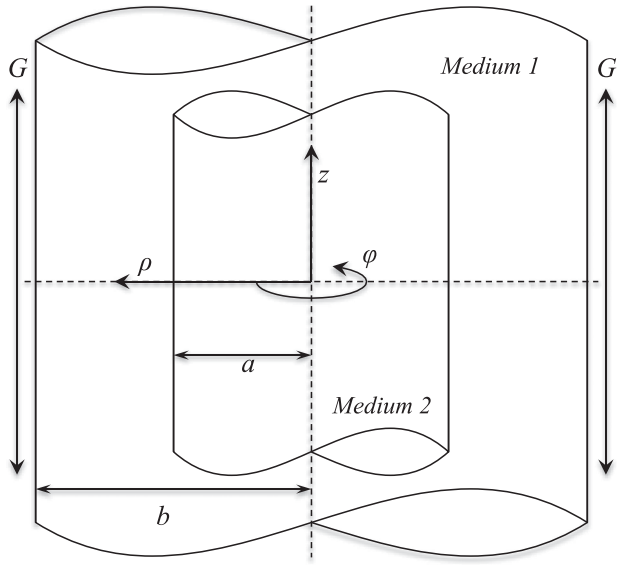

Fig. 1. Cylindrical media are referred to a cylindrical coordinate system (ρ, ϕ, z) with the z-axis coinciding with the axes of the media. Here a and b are the respective radii of medium 1 and 2, and G is the amplitude of the vertical oscillations.

II. Theory

A. Problem Formulation

Let there be given an infinitely long, rigid, circular cylindrical tube of inner radius, b, filled with an elastic solid, medium 1. Concentrically embedded therein is a circular cylindrical elastic solid, medium 2, with mechanical properties different from medium 1. This system is described by cylindrical coordinates (ρ, ϕ, z) [27], and shown in Fig. 1. The rigid tube harmonically oscillates along the z-axis and we assume medium 1 is in welded contact with both medium 2 and the oscillating wall. The displacement, $\vec{U}$, of both media satisfy the vector Helmholtz equation [28],

$$\alpha_i^2 \nabla\nabla\cdot\vec{U} - \beta_i^2 \nabla\times\nabla\times\vec{U} + \omega^2\vec{U} = 0 \tag{1}$$

where

$$\alpha_i^2 = (\lambda_i + 2\mu_i)\,\gamma_i^{-1}, \quad (i = 1, 2) \tag{2a}$$

and

$$\beta_i^2 = \mu_i \gamma_i^{-1}, \quad (i = 1, 2). \tag{2b}$$

Here α_i and β_i are the longitudinal and transverse wave speeds, respectively, the constants, λ_i and μ_i, are the Lame constants, and γ_i is the density of the material. We hold that $\lambda_i = (2\mu_i\nu)/(1-2\nu)$, where Poisson's ratio is $\nu = 0.4999998$ for both media. We choose that value for ν to satisfy the assumption that, like biological soft tissue or water-based tissue-like materials, the two media finite bulk moduli are about six orders of magnitude larger than their shear moduli. Finite-element simulations can be sensitive to small changes in ν as it approaches 0.5 (incompressibility). Here the index i is 1 or 2 to denote the medium, i.e.,

$$i = \begin{cases} 1, & \text{if } a < \rho \leq b \\ 2, & \text{if } 0 < \rho \leq a \end{cases}. \tag{3}$$

We suppress the harmonic time dependence, $e^{-i\omega t}$, throughout this study. The boundary condition at the outer surface of medium 1 is equality of tangential displacement of the wall and elastic medium,

$$u_1(\rho)|_{\rho=b} = G \tag{4}$$

where G is the amplitude of the forced oscillations. At the interface between media 1 and 2, the boundary conditions are equality of the tangential displacement and stress,

$$u_1(\rho)|_{\rho=a} = u_2(\rho)|_{\rho=a} \tag{5a}$$

and

$$\sigma_1(\rho)|_{\rho=a} = \sigma_2(\rho)|_{\rho=a}. \tag{5b}$$

The solution of (1) can be given as the sum of the longitudinal, $\vec{L}$, and transverse, $\vec{M}$ and $\vec{N}$, vector wave functions which are given as

$$\vec{L} = \nabla\Phi \tag{6a}$$

$$\vec{M} = \nabla \times \hat{e}\Psi \tag{6b}$$

$$\vec{N} = \beta_i^{-1}\nabla \times \nabla \times \hat{e}\mathrm{X} \tag{6c}$$

where Φ, Ψ, and X each solves the scalar Helmholtz equation,

$$\left(\nabla^2 + \left\{\alpha_i^{-2}, \beta_i^{-2}, \beta_i^{-2}\right\}\right)\{\Phi, \Psi, \mathrm{X}\} = 0 \tag{7}$$

and the vector, $\hat{e}$, depends on the coordinate system [28]. The components of displacement are: the displacement in medium 1 is the sum of the incident and scattered wave fields, $\vec{U}^{(i)}$ and $\vec{U}^{(s)}$, respectively, while the displacement in medium 2 is from the refracted wave field only, $\vec{U}^{(r)}$. We can write, then, the displacement as a piecewise continuous function throughout the entire domain, i.e.,

$$u(\rho) = \begin{cases} u_1(\rho) = \vec{U}^{(i)} + \vec{U}^{(s)}, & \text{if } a < \rho \leq b \\ u_2(\rho) = \vec{U}^{(r)}, & \text{if } 0 < \rho \leq a \end{cases}. \tag{8}$$

Due to the axial and longitudinal symmetry of our system, we are concerned with only the vertically-polarized transverse waves, i.e., $\vec{L} = \vec{M} = 0$ for all wave fields. The wave fields are, then, simply given as

$$\vec{U}^{\{(i),(s),(r)\}} = \vec{N}^{\{(i),(s),(r)\}}. \tag{9}$$

TABLE I
CONCENTRATIONS OF POLYMERS, IN PERCENT BY WEIGHT, IN THE TWO HYDROCOLLOID MEDIA

Medium	% by weight gelatin	% by weight agarose
1	4	0.75
2	1	0.4

In cylindrical cooordinates, $\hat{e}$ is the unit vector, $\hat{z}$, making the vector function [29]

$$\vec{N}^{\{(i),(s),(r)\}} = \frac{\beta_i}{\omega\rho}\frac{\partial}{\partial\rho}\left(\rho\frac{\partial \mathrm{X}^{\{(i),(s),(r)\}}}{\partial\rho}\right)\hat{z}. \tag{10}$$

We can calculate the relevant components of the stress tensor, $\sigma_{\rho z}$, directly from the displacement, given here as

$$\sigma_i = \mu_i\frac{\partial u_i(\rho)}{\partial\rho}, \quad (i = 1, 2). \tag{11}$$

B. Solutions

The potential functions are given by

$$\mathrm{X}^{\{(i),(s),(r)\}} = \{AJ_0(q_1\rho), BH_0(q_1\rho), CJ_0(q_2\rho)\} \tag{12}$$

where the wave number

$$q_i = \frac{\omega}{\beta_i}, \quad (i = 1, 2), \tag{13}$$

and A, B, and C are the unknown coefficients determined by satisfying the boundary conditions. Here J_0 and H_0 are the 0th-order cyllindrical Bessel and Hankel functions [30], respectively.

C. Boundary Conditions

Considering (12), (10), (9), and (8), the boundary conditions, (4) and (5a), become three equations through three unknowns, given in matrix form as

$$\begin{bmatrix} \varepsilon_{11} & \varepsilon_{12} & \varepsilon_{13} \\ \varepsilon_{21} & \varepsilon_{22} & \varepsilon_{23} \\ \varepsilon_{31} & \varepsilon_{32} & \varepsilon_{33} \end{bmatrix}\begin{bmatrix} A \\ B \\ C \end{bmatrix} = \begin{bmatrix} G \\ 0 \\ 0 \end{bmatrix}. \tag{14}$$

The elements of (14), $\varepsilon_{\mathrm{mn}}$, are given in Appendix A. Solving for A, B, and C, completely determines all wave fields, concluding the mathematical analysis. Expressions for A, B, and C are given in Appendix B. When a goes to zero, we get the limiting case of no heterogeniety which is the same as when $q_1 = q_2$.

III. METHOD

A. Phantom Construction

1) Matrix Preparation: The matrices of the inner and outer cylinders are hydrocolloids made from a mixture of agarose (SeaKem LE Agarose, Lonza, Rockland, ME) and food grade gelatin (Knox Original Unflavored Gelatine, Kraft Foods Group Inc., Northfield, IL, USA) in water. The concentrations of the separate media are summarized in Table I. Each hydrocolloid

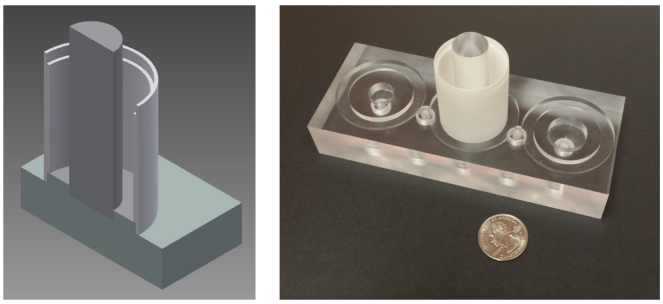

Fig. 2. Cut-away view of the assembly (left), and molding (right).

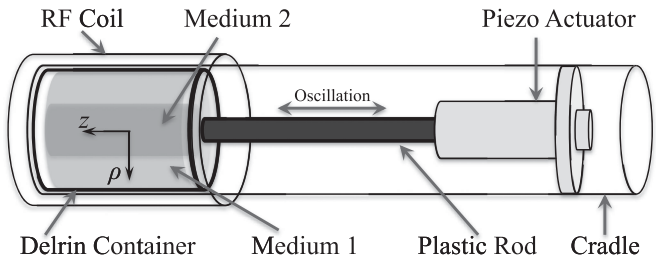

Fig. 3. Schematic diagram of the experimental setup.

was prepared by first sprinkling granulated gelatin into room temperature DI water which was then heated while stirred constantly. Once all the gelatin dissolved, agarose was then added. Heating and stirring continued until clarification, at $90\,^{\circ}$C. The molten gel was allowed to cool to about $40\,^{\circ}$C before being poured into the molding hydrocolloid.

2) Molding: To ensure concentricity between the two hydrocolloid solids, we designed and had custom-build a mold, depicted in Fig. 2, left and right, respectively, as a cut-away view and as it exists in the laboratory. On the bottom is a stage made of poly(methyl methacrylate) (PMMA) (Plexiglas, Rohn and Haas Company, Philadelphia, PA, USA) with a raised annular dais, in the center of which a removable PMMA rod tightly fits. Encircling the dais is the cylindrical container made of an acetyl resin (Delrin, DSM Engineering Plastic Products, Inc., Reading, PA, USA).

3) Phantom Assembly: The final assembly of the phantom is basically a two-step process: Step 1-the outer cylinder (medium 1), Step 2-the inner cylinder (medium 2). For medium 1, the delrin container is mounted on the dais and the acrylic rod is inserted in the depression. We then pour the $40\,^{\circ}$C molten medium 1 into the space between the delryn and PMMA, paying particular attention for any bubbles that might form. It is important that there be no bubbles—or any heterogeneity—within each medium as they would cause scattering and diffraction of the mechanical waves for which we do not account in our mathematical model. Air, especially, would be disruptive to the waves because fluids do not support shear waves, guaranteeing a mode conversion. Once the mold is filled, it is set aside and allowed to cool. We found that no sealant is necessary between the cylindrical container and dais. It is at this point when we prepare the hydrocolloid for medium 2, Section III-A1. Medium 1 will stick to the acetyl resin but not the PMMA; so, once it has solidified, we vertically pull the cylindrical container off the dais, sliding the medium 1 off the rod. Now begins step 2. First, we remove the rod from the dais. To ensure that the media are flush with each other, we stretch a piece of plastic paraffin film (Parafilm"M", Bemis Flexible Packaging, Neenah, WI, USA) over the dais to cover the depression before replacing the cylindrical container and medium 1 on the dais. Once affixed, we poured the molten medium 2 into the vacancy left by the rod. We then allow the entire body to cool to room temperature before removing it from the dais for scanning.

TABLE II
PARAMETERS FOR DATA ACQUISITION

TR	1 s
TE	28 ms
FOV	4 cm × 4 cm
Matrix size	128 × 128
Slice thickness	1 mm
MSG	30 G/cm

B. Experimental Setup

MR elastography experiments were performed at 9.4 T using a horizontal bore Agilent small-animal MR scanner (310/ASR, Agilent Technologies, Santa Clara, CA, USA) [20]. A 39-mm diameter quadrature RF coil was used inside a 60-mm diameter gradient coil with a maximum gradient of 1000 G/m. The gel-filled container was placed horizontally inside the center of the RF coil. The container was attached to a preloaded piezoactuator (p-840.1, PhysikInstrumente (PI) GmbH & Co. KG, Germany), which generates the transverse vibration motion (see Fig. 3). All phantoms were scanned at the excitation frequencies of 250, 500, 750, and 1000 Hz. This experimental setup establishes concentric wave patterns within the gel.

C. Data Acquisition

A customized spin-echo based MR elastography sequence with a sinusoidal motion-sensitizing gradient (MSG) was used for data acquisition, obtaining one axial slice and one coronal slice. The acquisition parameters, summarized in II, were as follows: repetition time (TR) = 1 s, echo time (TE) = 28 ms, field of view (FOV) = 4 cm × 4 cm, matrix size = 128 × 128, slice thickness = 1 mm, MSG = 30 G/cm.

The number of MSG cycles varied with the actuation frequency from 2 to 6 to accommodate constant TR/TE imaging parameters. In all scans, the MSG was applied along the principle direction of vibration in our experimental setup. Phase difference images were made from two acquisitions by inverting the polarity of the MSG. Eight time steps were acquired per actuation cycle.

D. Estimation of Shear Moduli, μ_i

To estimate the complex moduli of the two media, we fit the analytic solution for displacement in (8), $u(\rho)$, to the displacement data. We wrote a fitting algorithm in MATLAB

TABLE III
PARAMETERS FOR FEM

a	0.75 cm
b	1.5 cm
height	3 cm
degrees of freedom	50 586
no. of elements	12 496
max. element size	0.3 mm

(Math-Works, Inc., Natick, MA, USA) called data analysis and visualization toolbox (DeVIANT). It is an optimization that uses a global search algorithm to avoid any highly probable local minima. Within the global optimization toolbox of MATLAB, we preferred the MultiStart function to the GlobalSearch function because of the former is better as circumventing local minima. It is described in further detail in [24], and freely available as a standalone executable program at the Audible Human Project website: http://acoustics.mie.uic.edu/AHP/htdocs/default.php. Briefly, the data to which we fit the model is a linear profile taken from the experimental complex wave images, u_n, which includes and is normal to the z-axis and whose length is the diameter of the cylinder. We add some parameters to the model to take into account phase, θ, bias from compression wave, η, magnitude scale, s, and off-centering, δ. We express this as

$$\min_{\Psi} \sum_{n=-N}^{N} \| u_n - \hat{u}\left(\rho_n\right) \|^2 \tag{15}$$

where

$$\hat{u}(\rho) = s \times e^{i\theta} \times u(\rho_n + \delta) + \eta \tag{16}$$

and the set of parameters is $\Psi = \{\mu_1, \mu_2, \theta, \eta, s, \delta\}$. The chief difference in DeVIANT for this study is that we are finding the complex shear moduli of two different regions with a piecewise-continuous function, (8).

E. Forward Problem

Our analytic model assumes that the cylinders are infinitely long; i.e., we neglect edge effects from the top and bottom of the phantom. To validate our estimates, then, we created a two-dimensional, axisymmetric FEM in ANSYS (12.1 v, ANSYS, Inc. Pittsburg, PA, USA). We used a quadrilateral mesh of 12 496 elements and with a maximum element dimension of 0.3 mm, and with 50 586 degrees of freedom, summarized in Table III. We solved the forward problem using as inputs the parameters of the experimental procedures ($\omega = 2\pi f$, where $f = 250, 500, 750,$ and 1000 Hz., $a = 0.75$ cm, $b = 1.5$ cm, height$= 3$ cm) and fitting results (see Section IV).

IV. RESULTS

We scanned at four frequencies, 250, 500, 750, and 1000 Hz. These are reasonable upper and lower limits because vibrations at frequencies less than 250 Hz would yield wavelengths longer than the diameter of the phantom, making it difficult to see the agreement between model and experiment. Going higher then 1000 Hz would also obscure any agreement between theory and data because the attenuation of the mechanical waves would overcome the effect of geometric focusing in this geometry, i.e., we would have no discernible displacement save for at the radial periphery of the phantom. At each frequency, we fit the displacement to ten linear profiles taken from the displacement and, then, calculate the complex moduli from each profile. In Fig. 4, we show plots of the mean $\pm$ one standard deviation of the real (left) and imaginary (right) components of μ_1 (top) and μ_2 (bottom). All the moduli are numerically summarized in Table IV.

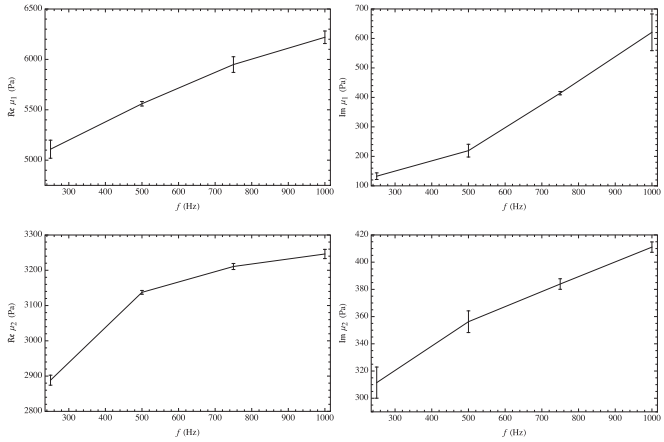

Fig. 4. Shear storage (left) and loss (right) moduli of Medium 1 (top) and Medium 2 (bottom). The error bars are one standard deviation from the mean.

TABLE IV
COMPLEX SHEAR MODULI, μ_1 AND μ_2, $\pm$ ONE STANDARD DEVIATION IN UNITS OF PA

f	$\mathfrak{Re}\mu_1$	$\mathfrak{Im}\mu_1$	$\mathfrak{Re}\mu_2$	$\mathfrak{Im}\mu_2$
250	5108 ± 90	133 ± 11	2888 ± 14	311 ± 11
500	5560 ± 22	219 ± 22	3137 ± 5	356 ± 8
750	5949 ± 78	414 ± 6	3210 ± 9	384 ± 4
1000	6219 ± 62	620 ± 15	3246 ± 13	411 ± 4

The frequency, f, is in Hz.

We can see a frequency dependence wherein the complex shear moduli of both media increase as does the frequency of the applied vibrations, in keeping with previously reported trends of hydrocolloids of gelatin [31] and agarose-gelatin mixtures [26]. To illustrate the frequency dependence from our results, we compare the means of μ_i from adjacent frequencies, e.g., $\mathfrak{Re}\mu_1 = 5108 \pm 90$ Pa at 250 Hz compared to $\mathfrak{Re}\mu_1 = 5560 \pm 22$ at 500 Hz, determining significance via the paired t-test [32]. In all cases, shear moduli significantly differed with frequency with $p < 0.001$.

The experimental (left) and simulated (right) wave images in the plane parallel to the z-axis and containing the origin for the scans at 250, 500, 750, and 1000 Hz are shown in Fig. 5(a), (b), (c), and (d), respectively. We can see close agreement between theory and data in all four frequencies. A more profound understanding of how our FEM matches the data is realized

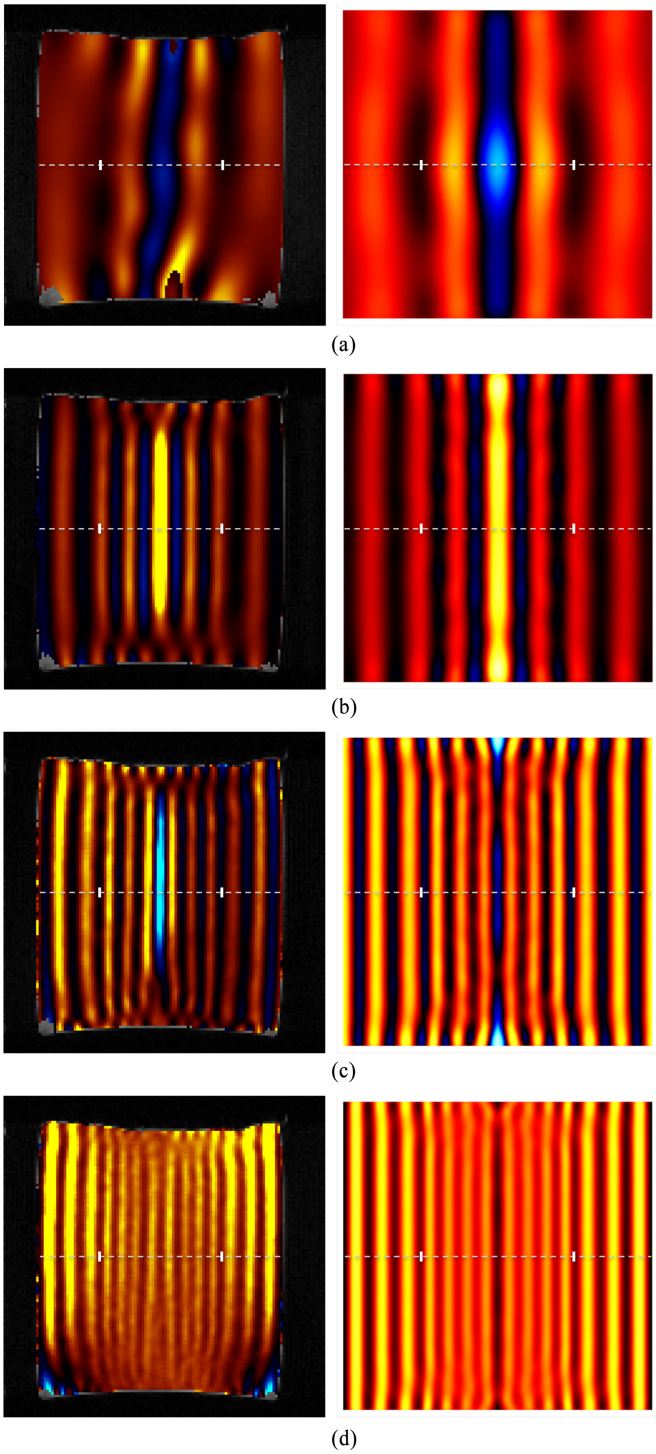

Fig. 5. Experimental (left) and FEM (right) wave fields through a plane parallel to the z-axis, containing the origin. The excitation frequencies 250, 500, 750, and 1000 Hz correspond to (a), (b), (c), and (d), respectively. The white tick marks indicate the interface between the two media, i.e., where $\rho = a$.

when we plot their linear profiles together, shown in Fig. 6(a), (b), (c), and (d) for frequencies, 250, 500, 750, and 1000 Hz, respectively. Finally, to validate our FEM, we plot it against our analytic solution, (8), in Fig. 7.

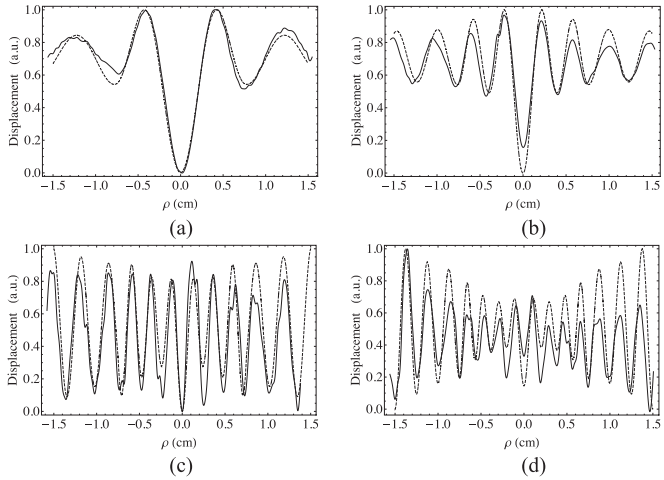

Fig. 6. Comparison of the FEM wave fields (dashed) to experimental (solid) displacements along a horizontal line through the fields in Fig. 5(a), (b), (c), and (d).

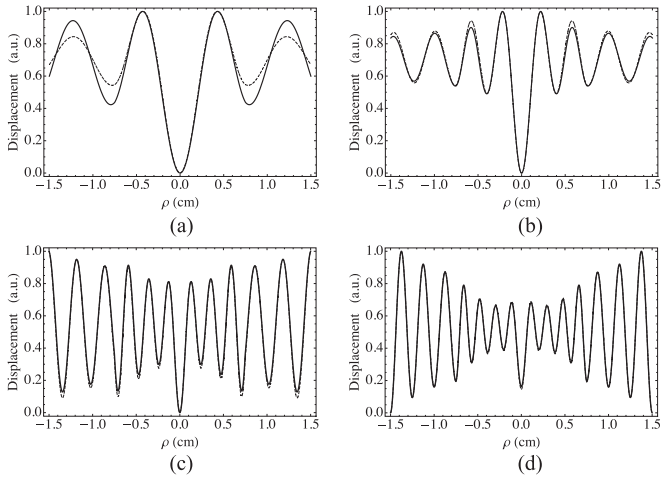

Fig. 7. Comparison of the FEM wave fields (dashed) in Fig. 6 to the analytic solution (solid) given in (8).

V. Discussion

The connectedness of a mechanical system is central to its internal operation as well as its response to external stimuli. In the context of MR elastography, we are concerned with the behavior of biologic materials through which mechanical energy is propagating. Ultimately this is a medical device, to be used on an organismic scale, e.g., human beings; so, the biomaterials in question will be found in a very complex network of interacting systems connected on many levels, e.g., electrically, chemically, hæmodynamically, and, of course, mechanically. The elastodynamic behavior of a material depends on its surroundings and biomaterials are no exception. It behoves us, then, to investigate not only the behavior of tissue-mimicking materials, but the behavior of said materials ensconced in a system-mimicking setting. To that end we have modeled, designed, built, and tested a multiply connected hydrogel phantom. We address the results in turn, considering their implications.

From the model fitting, we find that the complex shear moduli of the materials increase with the oscillatory frequency of the mechanical actuator. While, as noted in Section IV, this does generally follow reported trends of hydrogels, it is not clear how the specific composition of our gels informed the results. Obviously increasing the total colloid concentration increased the stiffness, but it is not clear what role the individual colloids had. Our mathematical model does not distinguish between the types of colloids or their chemical interactions or their molecular interconnectedness. Employing fractal models of polymers [33] might shed light here as could generalizing the calculus operations [34], [35].

In our forward modeling, we find close agreement between the theory and experiment. In the experimental images of Fig. 5(a), (b), (c), and (d), there appears to be a distortion in the wave field at the axial extremes. It is most pronounced in the lowest frequency, becoming progressively less so as the frequency goes up. Given the location, we assume this is an edge effect—waves scattered from the top and bottom surfaces—and, thus, why we used an FEM for the forward problem. By inspection of Fig. 5(b), (c), and (d), one can easily see that the wave fields are straight, up and down, in the vertical center of the phantom, both in the theory and experiment. This is because of the preferential attenuation of high-frequency waves in viscoelastic media. The waves scattered from the top and bottom surfaces are decreasingly detectible at the vertical center of the phantom as the excitation frequency goes up. We can see this even more apparently in the comparison of the line profiles of the FEM to those of the analytic solution, shown in Fig. 7. The two profiles are in near perfect agreement at $f = 1000$ Hz, progressively falling out thereof as the f goes down. Moreover, this trend seems to be even more pronounced in the periphery of the phantom which supports the notion that it is due to the attenuation of edge effect waves. The periphery of the phantom is Medium 1 which has four times the gelatin concentration and just under twice the agarose concentration of Medium 2, making Medium 1 necessarily stiffer, thus, less dampening than Medium 2. In other words, the radial center of the phantom is too soft for even the 250-Hz edge effect waves to be detectible at the vertical center. All of this highlights the major flaw with our closed form analytic model, i.e., the assumption that the cylinders are infinite in length. Our FEM seems to capture the apparent edge effects but not perfectly, implying that there is more at work than yet described mathematically. One very real possibility is the existence of a third cylindrical layer. We tried to switch the two media, i.e., make the inner cylinder out of the stiffer medium 1 and vice versa, but the softer hydrocolloid would not stick at all to the resin shell. This is likely due to the reduced gelatin content, because the two media still stuck to each other. Perhaps also the interface between the two media is not as stark as our mathematical model assumes. We speculate that mixing or, at least, diffusion happens while the second hydrocolloid cools, transitioning from sol to gel. Immediately upon touching the first medium, the heat of the second will melt a thin layer of the first, forming an intermediate layer. Having a different colloid concentration from the layers on either side, this layer would have different mechanical properties from the other layers, ergo its own two wave fields and unknown coefficients as well as change the expressions for the waves of the original media. This speaks to the point of our study, that the increasing precision of imaging modalities demands more careful and precise tools of validation and verification. This study features novel mathematical modeling but also deigned to showcase our phantom construction techniques and the exceptional care required in such highly determined systems.

Finally, it is noticeable in the planar images and very clear in the linear profiles that, despite our best efforts in phantom construction, we have not achieved perfect axial symmetry at all frequencies. It is most apparent in the linear profile of 1000 Hz in Fig. 6(d). Note, however, that the amplitude seems to be equal but opposite across the origin, i.e., it is very high on the left side and very low on the right side. It is possible that this is due to the experimental setup and not actually the phantom construction. We use the same protocol as that described in [20]. The asymmetric displacement is likely due to the horizontal positioning shown in Fig. 3, of the phantom, causing unequal contact force between the gel and resin container. The gel on the side facing down would be under the weight of the entire phantom pushing it down as well as the cohesion of the gel to create a shear force, while the side facing up would have merely the cohesion of the gel.

VI. Conclusion

We applied MRE to our custom-designed multiply connected hydrogel phantom. We derived a closed form analytic solution of the displacement therein which we fit to the wave field data, thus estimating its mechanical properties which became the input parameters of our forward FEM. We showed that the edge effects can affect the wave field deep in axial center of the phantom if the vibrational frequency is low enough or the material is stiff enough that those waves are not attenuated. Such phenomena, therefore, must be considered when deriving analytic models of geometrically amenable objects. Analytic approaches generally can boast higher speed, precision, and stability than those numeric. We have used out analytic model to better understand both out experimental work and finite-element simulation. Indeed, both analytic and finite-element analysis can help us identify shortcomings of conventional reconstruction algorithms, e.g., LFE, which fail to account for boundary effects and mode conversion and whose results can be dramatically biased by filtering choices. Further modeling and experimental studies are needed to determine the optimal ranges of relevant parameters, e.g., length, material stiffness, excitation frequency, that confounding phenomena like edge effects are ameliorated.

Appendix A
Matrix Elements $\varepsilon_{\mathrm{mn}}$

After considerable algebraic simplification, the elements of (14), $\varepsilon_{\mathrm{mn}}$, are given here as

$$\varepsilon_{11} = \varepsilon_{21} = -q_1 J_0(bq_1) \tag{A.17a}$$

$$\varepsilon_{13} = 0 \tag{A.17b}$$

$$\varepsilon_{12} = \varepsilon_{22} = -q_1 H_0(bq_1) \quad \text{(A.17c)}$$

$$\varepsilon_{23} = -q_2 J_0(bq_2) \quad \text{(A.17d)}$$

$$\varepsilon_{31} = -\mu_1 q_1^2 J_1(aq_1) \quad \text{(A.17e)}$$

$$\varepsilon_{32} = -\mu_1 q_1^2 H_1(aq_1) \quad \text{(A.17f)}$$

$$\varepsilon_{33} = -\mu_2 q_2^2 J_1(aq_2). \quad \text{(A.17g)}$$

Appendix B
Expansion Coefficients A, B, and C

The expansion coefficients A, B, and C are too cumbersome to write out completely. Instead, they are given here in parametric from, i.e.,

$$A = \frac{Gq_1\mu_1 c}{q_1 d} \quad \text{(B.18a)}$$

$$B = \frac{Gq_2\mu_2 e}{q_1 d} \quad \text{(B.18b)}$$

$$C = \frac{2iG\mu_1}{\pi a q_2 f} \quad \text{(B.18c)}$$

where

$$d = q_1\mu_1 J_0(aq_1)c + q_2\mu_2 J_1(aq_2)g \quad \text{(B.19a)}$$

$$f = q_1\mu_1 J_0(aq_2)h + q_2\mu_2 J_1(aq_2)j \quad \text{(B.19b)}$$

and where

$$c = H_1(aq_1)J_0(aq_2) - H_0(aq_1)J_1(aq_2) \quad \text{(B.20a)}$$

$$e = J_0(aq_1)J_1(aq_2) - J_1(aq_1)J_0(aq_2) \quad \text{(B.20b)}$$

$$g = H_0(aq_1)J_0(bq_1) - J_0(aq_1)H_1(bq_1) \quad \text{(B.20c)}$$

$$h = H_1(aq_1)J_0(bq_1) - J_1(aq_1)H_0(bq_1) \quad \text{(B.20d)}$$

$$j = J_0(aq_1)H_0(bq_1) - H_0(aq_1)J_0(bq_1). \quad \text{(B.20e)}$$

References

[1] H. Xie *et al.*, "Correspondence of ultrasound elasticity imaging to direct mechanical measurement in aging DVT in rats," *Ultrasound Med. Biol.*, vol. 31, no. 10, pp. 1351–1359, Oct. 2005.

[2] R. Muthupillai *et al.*, "Magnetic resonance elastography by direct visualization of propagating acoustic strain waves," *Science*, vol. 269, no. 29, pp. 1854–1857, Sep. 1995.

[3] R. Muthupillai and R. L. Ehman, "Magnetic resonance elastography," *Nat. Med.*, vol. 2, no. 5, pp. 601–603, May 1996.

[4] D. B. Plewes, C. L. Walker, and F. S. Foster, "Quantitative magnetic resonance imaging of ultrasound fields," in *Proc. IEEE Ultrasonics Symp.*, Toronto, ON, Canada, 1997, pp. 1297–1300

[5] C. L. Walker *et al.*, "Magnetic resonance imaging of ultrasonic fields," *Ultrasound Med. Biol.*, vol. 24, no. 1, pp. 137–142, Jan. 1998.

[6] M. M. Doyley, "Model-based elastography: A survey of approaches to the inverse elasticity problem," *Phys. Med. Biol.*, vol. 57, no. 3, pp. R35–R73, Feb. 2012.

[7] D. H. Everett, *Basic Principles of Colloid Science*. London, U.K.: Royal Society of Chemistry, 1992, pp. 185–190, ch. 13.

[8] P. R. Perriñez *et al.*, "Modeling of soft poroelastic tissue in time-harmonic MR elastography," *IEEE Trans. Biomed. Eng.*, vol. 56, no. 3, pp. 598–608, Mar. 2009.

[9] S. F. Othman *et al.*, "Microscopic magnetic resonance elastography (μMRE)," *Magn. Res. Med.*, vol. 54, no. 3, pp. 605–615, Sep. 2005.

[10] S. F. Othman *et al.*, "Error propagation model for microscopic magnetic resonance elastography shear-wave images," *Magn. Res. Imag.*, vol. 25, no. 1, pp. 94–100, Jan. 2007.

[11] C. Amador *et al.*, "Shear elastic modulus estimation from indentation and SDUV on gelatin phantoms," *IEEE Trans. Biomed. Eng.*, vol. 58, no. 6, pp. 1706–1714, Jun. 2011.

[12] X. Zhang *et al.*, "Comparison of the surface wave method and the indentation method for measuring the elasticity of gelatin phangoms of different concentrations," *Ultrasonics*, vol. 51, no. 2, pp. 157–164, Feb. 2011.

[13] K. Riek *et al.*, "Wide-range dynamic magnetic resonance elastography," *J. Biomech.*, vol. 44, no. 7, pp. 1380–1386, Apr. 2011.

[14] Y. A. Petrov *et al.*, "Multi-frequency inversion in Rayleigh damped magnetic resonance elastography," *Biomed. Signal Proces.*, vol. 13, pp. 270–281, Sep. 2014.

[15] A. H. Henni *et al.*, "Three-dimensional transient and harmonic shear-wave scattering by a soft cylinder for dynamic vascular elastography," *J. Acoust. Soc. Amer.*, vol. 124, no. 4, pp. 2394–2405, Oct. 2008.

[16] C. Schmitt *et al.*, "Ultrasound dynamic micro-elastography applied to the viscoelastic characterization of soft tissues and arterial walls," *Ultrasound Med. Biol.*, vol. 36, no. 9, pp. 1492–1503, Sep. 2010.

[17] C. Schmitt *et al.*, "Characterization of blood clot viscoelasticity by dynamic ultrasound elastography and modeling of the rheological behavior," *J. Biomech.*, vol. 44, no. 4, pp. 622–629, Feb. 2011.

[18] M. M. Doyley *et al.*, "The performance of steady-state harmonic magnetic resonance elastography when applied to viscoelastic materials," *Med. Phys.*, vol. 37, no. 8, pp. 3970–3979, Aug. 2010.

[19] E. C. Qin *et al.*, "Combining MR elastography and diffusion tensor imaging for the assessment of anisotropic mechanical properties: A phantom study," *J. Magn. Reson. Imag.*, vol. 37, no. 1, pp. 217–226, Jan. 2013.

[20] Z. Yin *et al.*, "Simultaneous MR elastography and diffusion acquisitions: diffusion-MRE (dMRE)," *Magn. Reson. Med*, vol. 71, no. 5, pp. 1682–1688, May. 2014.

[21] H. Knutsson *et al.*, "Local multiscale frequency and bandwidth estimation," in *Proc. IEEE Int. Conf. Imag. Processing*, Chicago, IL, USA, 1994, pp. 36–40.

[22] A. A. Khan *et al.*, "Localized elastography map of human cornea through surface vibrations," in *Proc. Int. Mech. Eng. Cong. Exp.*, San Diego, CA, USA, 2013, pp. V03BT03A049.

[23] T. K. Yasar *et al.*, "Taking MR elastography (MRE) to the microscopic scale (μMRE)," in *Proc. IEEE Int. Symp. Biomed. Imag.: Nano Macro*, Chicago, IL, USA, 2011, pp. 1618–1623.

[24] T. K. Yasar *et al.*, "Wideband MR elastography for viscoelasticity model identification," *Magn. Reson. Med*, vol. 70, no. 2, pp. 479–489, Aug. 2013.

[25] Y. Liu *et al.*, "Ultra wideband (0.5–16kHz) MR elastography for robust shear viscoelasticity model identification," *Phys. Med. Biol.*, vol. 59, no. 24, pp. 7717–7734, Dec. 2014.

[26] R. J. Okamoto *et al.*, "Viscoelastic properties of soft gels: comparison of magnetic resonance elastography and dynamic shear testing in the shear wave regime," *Phys. Med. Biol.*, vol. 56, no. 19, pp. 6379–6400, Oct. 2011.

[27] P. H. Moon and D. E. Spencer, *Field Theory Handbook: Including Coordinate Systems, Differential Equations and Their Solutions*. New York, NY, USA: Springer, 1961, pp. 12–17.

[28] P. M. Morse and H. Feshbach, *Methods of Theoretical Physics*. New York, NY, USA: McGraw-Hill, 1953, ch. 13, pp. 1763–1791.

[29] Y. -H. Pao and C. -C. Mow, *Diffraction of Elastic Waves and Dynamic Stress Concentrations*. New York, NY, USA: Crane, Russak & Company, Inc., 1973, pp. 601–612, ch. 6.

[30] W. W. Bell, *Special Functions for Scientists and Engineers*. New York, NY, USA: Dover, 2004, pp. 42–155, ch. 4.

[31] J. L. Doublier *et al.*, "Viscoelastic properties of food gels," in *Viscoelastic Properties of Food*, M. A. Rao, and J. F. Steffe, Eds. London, U.K.: Elsevier, 1992, pp. 371–434, ch. 14.

[32] J. M. Cameron, "Stastics," in *Fundamental Formulas of Physics*, D. H. Menzel, Ed. New York, NY, USA: Dover, 1960, pp. 107–140, ch. 2.

[33] M. Muthukumar, "Dynamics of polymeric fractals," *J. Chem. Phys.*, vol. 83, no. 6, pp. 3161–3168, Sep. 1985.

[34] R. L. Magin, "Fractional calculus models of complex dynamics in biological tissues," *Comput. Math. Appl.*, vol. 59, no. 5, pp. 1586–1593, Mar. 2010.

[35] R. L. Magin, *Fractional Calculus in Bioengineering*. Redding, CT, USA: Belgell House, 2006.

Benjamin L. Schwartz received the B.S.E. degree in bioengineering from Arizona State University, Tempe, AZ, USA, in 2006, the M.S. degree in bioengineering from the University of Vermont, Burlington, VT, USA, in 2009, and the Ph.D. degree in bioengineering from the University of Illinois at Chicago, Chicago, IL, USA in 2014.

His research interest include analytic methods of mathematic modeling of biomedical phenomena.

Ziying Yin received the B.S. degree in biomedical engineering in 2006, and the M.S. degree in computer application and technology in 2008 from Beijing Jiaotong University, Beijing, China. She received the Ph.D. degree in bioengieering from University of Illinois at Chicago, Chicago, IL, USA, in 2014.

She is currently a Research Fellow in the Department of Radiology, Mayo Clinic, Rochester, MN, USA. Her research mainly include the development and application of magnetic resonance elastography techniques.

Temel K. Yaşar received the B.S. and M.S. degrees in electrical engineering in 2002 and 2006, respectively, from Middle East Technical University, Ankara, Turkey, and Ph.D. degree in mechanical engineering in 2014 from University of Illinois at Chicago, Chicago, IL, USA.

He completed his post-doctoral studies at Mt. Sinai Translational and Molecular Imaging Institute. His research interest include advanced Magnetic Resonance Elastography techniques in preclinical and clinical MRI systems.

Yifei Liu received the B.S. degree in mechanical engineering from Donghua University, Shanghai, China, in 2002. She received the M.S. degree in 2010 and Ph.D. degree in 2015 from the Department of Mechanical and Industrial Engineering, University of Illinois at Chicago, Chicago, IL, USA.

She is currently an MR Lead System Engineer of Image Quality in GE Healthcare, Chalfont, U.K. She was with OptiWorks(Shanghai) Inc. as a Mechanical Engineer for six years. Her research interest includes development of magnetic resonance elastography (MRE) technique, numerical calculation in MRE, finite element modeling and analysis, and magnetic resonance image quality improvement.

Altaf A. Khan received his B.S. degree in Mechanical Engineering in 2010 from University of Illinois at Chicago, Chicago, IL, USA, and is currently working toward the Ph.D. degree in mechanical engineering there, too.

He has worked extensively with vibration through elastic and viscoelastic materials such as human and animal tissue. He uses different imaging techniques, including magnetic resonance elastography and scanning laser doppler vibrometry. He is currently studying the affects of wave motion across the fingertip for sensational perception.

Allen Q. Ye received the Bachelor's degree in biomedical engineering from Case Western Reserve University, Cleveland, OH, USA, in 2009, and is currently working toward the M.D. and Ph.D. degrees at University of Illinois at Chicago, Chicago, IL, USA.

His research interests include magnetic resonance, diffusion, and neuroimaging.

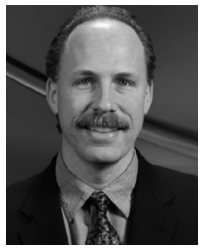

Thomas J. Royston received the Ph.D. degree in mechanical engineering from the Ohio State University, Columbus, OH, USA, in 1995.

He is a Professor and Head of the Richard and Loan Hill Department of Bioengineering, University of Illinois at Chicago, Chicago, IL, USA.

Prof. Royston's research in acoustics and vibrations has been supported by grants from the NSF, NIH, ONR, and DOE. He received the US NSF Career Award (1998) and the Acoustical Society of Americas R. Bruce Lindsay Award (2002). He is a Fellow of the American Society of Mechanical Engineers (2007). In 2014, he was recognized by NIH with the NIBIB New Investigator Award for his work on The Audible Human Project.

Richard L. Magin (M'69–SM'81–F'96) received the B.S. and M.S. degrees in physics from the Georgia Institute of Technology, Atlanta, GA, USA, in 1969 and 1972, respectively. He received the Ph.D. degree in biophysics from the University of Rochester, Rochester, NY, USA, in 1976.

He is currently a Distinguished Professor of bioengineering at the University of Illinois at Chicago, Chicago, IL, USA. His research interests include the application of magnetic resonance imaging in science and engineering. He served as an Editor for the Critical Reviews in Biomedical Engineering (2005–2010).

Prof. Magin is a Member of the Biomedical Engineering Society and of the International Society of Magnetic Resonance in Medicine. He is a Fellow of the American Institute for Medical and Biological Engineering. In 2005, he received a Fulbright Award for research and teaching in Kosice, Slovakia.